doi:10.1093/brain/awm335 *Brain* (2008), **131**, 352–367

OPA1 mutations associated with dominant optic atrophy impair oxidative phosphorylation and mitochondrial fusion

Claudia Zanna,[1,*] Anna Ghelli,[1,*] Anna Maria Porcelli,[1] Mariusz Karbowski,[2] Richard J. Youle,[2] Simone Schimpf,[3] Bernd Wissinger,[3] Marcello Pinti,[4] Andrea Cossarizza,[4] Sara Vidoni,[1] Maria Lucia Valentino,[5] Michela Rugolo[1] and Valerio Carelli[5]

[1]Dipartimento di Biologia Evoluzionistica Sperimentale, Università di Bologna, Italy, [2]Biochemistry Section, National Institute of Neurological Disorders and Stroke, National Institutes of Health, Bethesda, MD, USA, [3]Molecular Genetics Laboratory, University Eye Hospital, Tuebingen, Germany, [4]Dipartimento di Scienze Biomediche, Sezione di Patologia Generale, Università di Modena e Reggio Emilia and [5]Dipartimento di Scienze Neurologiche, Università di Bologna, Italy

[*]These authors contributed equally to this work.

Correspondence to: Dr Claudia Zanna, Dipartimento di Biologia Evoluzionistica Sperimentale, Università di Bologna, Via Irnerio 42, 40126 Bologna, Italy
E-mail: zanna@alma.unibo.it

Dominant optic atrophy (DOA) is characterized by retinal ganglion cell degeneration leading to optic neuropathy. A subset of DOA is caused by mutations in the *OPA1* gene, encoding for a dynamin-related GTPase required for mitochondrial fusion. The functional consequences of *OPA1* mutations in DOA patients are still poorly understood. This study investigated the effect of five different *OPA1* pathogenic mutations on the energetic efficiency and mitochondrial network dynamics of skin fibroblasts from patients. Although DOA fibroblasts maintained their ATP levels and grew in galactose medium, i.e. under forced oxidative metabolism, a significant impairment in mitochondrial ATP synthesis driven by complex I substrates was found. Furthermore, balloon-like structures in the mitochondrial reticulum were observed in galactose medium and mitochondrial fusion was completely inhibited in about 50% of DOA fibroblasts, but not in control cells. Respiratory complex assembly and the expression level of complex I subunits were similar in control and DOA fibroblasts. Co-immunoprecipitation experiments revealed that OPA1 directly interacts with subunits of complexes I, II and III, but not IV and with apoptosis inducing factor. The results disclose a novel link between OPA1, apoptosis inducing factor and the respiratory complexes that may shed some light on the pathogenic mechanism of DOA.

Keywords: OPA1; DOA; oxidative phosphorylation; mitochondrial fusion; AIF

Abbreviations: AIF = apoptosis inducing factor; DMEM = Dulbecco's modified Eagle's medium; mito-PAGFP = mitochondrial matrix-targeted photoactivable green fluorescent protein; mtDNA = mitochondrial DNA; MTT = 3-[4,5-dimethylthiazol-2-yl]-2,5-diphenyl tetrazolium bromide; RGC = retinal ganglion cell

Received July 27, 2007. Revised December 18, 2007. Accepted December 19, 2007

Introduction

Mitochondrial hereditary optic neuropathies, the most common being Leber's hereditary optic neuropathy, are characterized by a selective degeneration of retinal ganglion cells (RGCs), leading to optic atrophy and blindness (Carelli *et al*., 2004). The Kjer-type dominant optic atrophy (DOA) (Kjer, 1959) has recently been added to the list of mitochondrial optic neuropathies. A subset of DOA cases has been associated with heterozygous mutations in the *OPA1* gene located on chromosome 3q28-q29 (Alexander *et al*., 2000; Delettre *et al*., 2000). This gene encodes a dynamin-related GTPase, which is targeted to mitochondria by an N-terminus import sequence motif and is anchored to the inner membrane facing the intermembrane space (Olichon *et al*., 2002). The OPA1 protein structure includes a transmembrane domain, a GTPase domain, a middle

domain and C-terminal coiled-coil domain proposed to be a GTPase effector domain (see http://lbbma.univ-angers.fr). Eight OPA1 mRNA isoforms resulting from alternative splicing have been described. These are variably expressed in different tissues, with the highest levels being found in retina, brain, testis, heart and muscle (Delettre *et al.*, 2001). Furthermore, the different isoforms seem to be related to distinct conserved OPA1 functions (Olichon *et al.*, 2007*a*).

To investigate OPA1 function at the cellular level, gene expression was downregulated by RNA interference in HeLa cells. This led to fragmentation of the mitochondrial network, loss of mitochondrial membrane potential and drastic disorganization of the cristae. Furthermore, spontaneous release of cytochrome c and caspase-dependent activation of the apoptotic cascade were observed in this experimental model (Olichon *et al.*, 2003). A quantitative mitochondrial fusion assay was used to demonstrate that OPA1 protein downregulation caused a complete inhibition of mitochondrial fusion (Lee *et al.*, 2004). Therefore, it has been proposed that OPA1, like its yeast homologue Mgm1p (Sesaki *et al.*, 2003), is involved in the regulation of mitochondrial dynamics and the maintenance of structural integrity of the cristae (Griparic *et al.*, 2004; Chen *et al.*, 2005). A recent study emphasized the role of OPA1 in cristae remodelling as a function independent from mitochondrial fusion, directly involved in regulating the apoptotic process through the control of cytochrome c redistribution (Frezza *et al.*, 2006).

Over 90 *OPA1* gene mutations have been described to date (Olichon *et al.*, 2006). These mutations may be substitutions, deletions or insertions and they are spread throughout the coding region of the gene, most of them being localized to the GTPase and the GED domains. The c.2708delTTAG frameshift-inducing microdeletion in the GED domain seems to be the most common in patients of European descent (see http://lbbma.univ-angers.fr).

The functional consequences of *OPA1* mutations in DOA patients have been poorly investigated. One recent study using phosphorus MR spectroscopy to assess calf muscle oxidative metabolism in patients carrying the c.2708delTTAG microdeletion, showed a subclinical defect in oxidative phosphorylation (Lodi *et al.*, 2004). This observation was reinforced by biochemical investigations in fibroblasts carrying the severe *OPA1* R445H mutation, where an oxidative phosphorylation defect was detected together with a significantly reduced rate of ATP synthesis compared to controls (Amati-Bonneau *et al.*, 2005). The R445H mutation, identified in multiple families, is associated with a complex clinical phenotype characterized by DOA, sensorineural deafness and in a few cases adjunctive myopathic features including ptosis and progressive external ophthalmoplegia (Payne *et al.*, 2004). Recently, the R445H mutation, as well as other mis-sense mutations at specific sites involving the GTPase domain of *OPA1*, have all been linked to mitochondrial DNA (mtDNA) instability and accumulation of multiple deletions in skeletal muscle (Amati-Bonneau *et al.*, 2007; Hudson *et al.*, 2007). Furthermore, another study reported a slight decrease in the number of mtDNA copies per cell in leucocytes from DOA patients with *OPA1* mutations (Kim *et al.*, 2005). Thus, *OPA1* also seems to be involved in mtDNA stability and possibly maintenance.

The present study undertook a comprehensive investigation of skin fibroblasts derived from DOA patients carrying the common c.2708delTTAG microdeletion and four other pathogenic mutations in the *OPA1* gene, all of which are predicted to truncate the protein product. The mitochondrial network morphology and ultrastructure, mitochondrial fusion and oxidative phosphorylation were significantly affected in DOA fibroblasts. Furthermore, we show that OPA1 physically interacts with different respiratory complex subunits and with apoptosis inducing factor (AIF), suggesting a possible mechanism for DOA pathophysiology.

Material and Methods

Materials

3-(4,5-Dimethylthiazol-2-yl)-2,5-diphenyltetrazolium bromide (MTT), tert butylhydroperoxide (t-BH), ATP and ATP monitoring kit were purchased from Sigma (Milan, Italy). Hoechst-33342 was from Calbiochem (La Jolla, CA, USA) and Mitotracker Red from Molecular Probes (Eugene, OR, USA). The antibodies used were as follows: anti-OPA1 (BD Bioscience Pharmingen, Milan, Italy), anti-mitofusin-1 (Abnova, Taipei, Taiwan), anti-DRP1 (Santa Cruz, CA, USA), anti-β-tubulin (Sigma), anti-AIF (Santa Cruz), anti-porin, anti-NDUFA9, anti-ND6 and anti-NDUFB6 subunits of complex I, anti-FP subunit of complex II, anti-core II subunit of complex III and anti-subunit I of complex IV (Molecular Probes). Secondary antibodies were from Jackson ImmunoResearch Europe Ltd (Soham, Cambridgeshire, UK).

OPA1 sequence analysis of DOA patients

For the *OPA1* mutation analysis genomic DNA was amplified by PCR with sense and anti-sense primers specific for the 30 previously described exons (Pesch *et al.*, 2001). PCR products were purified by ExoSAP treatment (Amersham, Munich, Germany) and sequenced employing BigDye Terminator chemistry (Applied Biosystems, Weiterstadt, Germany). Sequencing products were separated on an ABI 3100 DNA Sequencer and the data were assessed manually and using alignment tools. Total RNA was isolated from whole blood using the PAXgene Blood RNA system (Quiagen, Hilden, Germany). Single-stranded cDNA was synthesized applying the SuperScript First-Strand Synthesis System (Invitrogen, Carlsbad, CA) and overlapping fragments of the *OPA1* cDNA were amplified by PCR prior to direct DNA sequencing as described previously (Schimpf *et al.*, 2006).

Cells and culture conditions

Skin fibroblasts were derived, following informed consent, from five healthy donors, five DOA patients from two unrelated families with the c.2708delTTAG deletion, two patients with the c.2819-2A>C mutation and one patient with each of the other mutations (see the Results section).

Fibroblasts were grown in DMEM medium supplemented with 10% foetal bovine serum (FBS), 2 mM L-glutamine and antibiotics. The mtDNA-lacking 143B206 Rho0 cells and the osteosarcoma-derived 143B.TK-parental cells (a kind gift from Martinuzzi, King and Attardi) were grown in the same DMEM medium containing 50 μg/ml uridine or 0.1 mg/ml bromodeoxyuridine, respectively. For the experiments, fibroblasts were grown in DMEM glucose medium or DMEM glucose-free medium containing 5 mM galactose, 5 mM pyruvate (DMEM galactose medium).

Western blotting and immunoprecipitation

10^6 cells were resuspended in 0.1 ml of RIPA buffer (50 mM Tris–Cl pH 7.6, 150 mM NaCl, 1% NP-40, 1% NaDOC, 0.1% SDS, 5 mM EDTA, 100 μl/ml of protease inhibitor cocktail), sonicated and centrifuged at 10 000 *g*. The protein content of the supernatant (cell lysates) was determined according to Bradford (Bradford, 1976). Mitochondria were isolated from 4×10^6 fibroblasts by standard differential centrifugation. Proteins (30 μg) were separated by 8% SDS–PAGE and transferred onto a nitrocellulose membrane (Bio-Rad, Hertfordshire, UK). Primary antibodies were visualized using horseradish peroxidase-conjugated secondary antibodies. Signals were detected using ECL (Amersham). Densitometry was performed with a Fluo-2 MAX Multimager system (Bio-Rad).

For immunoprecipitation experiments, cell lysates (200 μg) were incubated in RIPA buffer and mixed with anti-OPA1 or anti-AIF antibodies at 4°C for 2 h. Protein A-Sepharose (Sigma) was then added. Precipitates were used for western blot analysis.

Blue native electrophoresis

Isolated mitochondria were solubilized using 0.5% lauryl maltoside (Sigma), and proteins were loaded on a linear 5–12% gradient polyacrylamide gel (Nijtmans *et al.*, 2002).

Cell viability and ATP assays

Cell viability was determined with the MTT assay (Ghelli *et al.*, 2003). ATP was measured by using the luciferin/luciferase assay (Zanna *et al.*, 2005).

Mitochondrial ATP synthesis

Mitochondrial ATP synthesis driven by complex I and II substrates was determined in digitonin-permeabilized fibroblasts, exactly as previously reported (Bonora *et al.*, 2006). ATP synthesis through glycerol 3-phosphate dehydrogenase (mGPD) was determined in the presence of 2 μg/ml rotenone and 25 mM glycerol 3-phosphate. Citrate synthase activity was measured as described in (Srere, 1969).

Nuclear and mitochondrial morphology

Nuclear and mitochondrial morphology was assessed after cell staining with 2 μg/ml Hoechst and 10 nM Mitotracker for 30 min at 37°C. Fluorescence was visualized with a digital imaging system using an inverted epifluorescence microscope with 63X/1.4 oil objective (Diaphot, Nikon, Japan). Images were captured with a back-illuminated Photometrics Cascade CCD camera system (Roper Scientific, Tucson, AZ, USA) and Metamorph acquisition/analysis software (Universal Imaging Corp., Downingtown, PA, USA).

Analysis and quantification of mitochondrial fusion

Cells were transfected with 1 μg of mitochondrial matrix-target photoactivable green fluorescent protein (mt-PAGFP) (Karbowski *et al.*, 2004) and incubated in DMEM-glucose or DMEM-galactose medium for 24 h. Images were captured with an LSM 510 confocal microscope (Carl Zeiss MicroImaging, Inc.) using a 63×1.4 NA Apochromat objective. The excitation and photoactivation wavelengths for mito-PAGFP were 488 nm and 413 nm, respectively. Regions of interest were selected and series of *z*-sections from the top to the cell bottom with intervals between the sections set to 0.5–0.75 μm were irradiated with 413-nm light. Images were captured immediately after photoactivation (0 min) and after 30 and 60 min. Mitochondrial fusion was calculated by obtaining the ratio between the number of pixels in the fluorescent area and the total cell number of pixels using the Volocity program. Data were exported to Microsoft Excel and converted into graphs.

Quantification of mtDNA

DNA was isolated using QIAmp DNA Blood Mini kit (Qiagen, Valencia, CA). The cell content of mtDNA was determined by double-competitive polymerase chain reaction (Cossarizza *et al.*, 2003).

Transmission electron microscopy

Fibroblasts grown in DMEM-glucose or DMEM-galactose medium were fixed with 4% paraformaldehyde. Thin sections were examined on a Jeol 1200 EXII TEM.

Statistical analysis

The data were analysed using the Student's *t*-test, unless otherwise indicated. Only values of $P < 0.05$ were considered significant.

Results

Energetic competence of fibroblasts with *OPA1* mutations

We studied fibroblasts derived from 10 patients carrying *OPA1* mutations. The localization of these mutations in the *OPA1* gene is reported in Fig. 1A. We also studied fibroblasts from five healthy donors. Five patients carried the frameshift c.2708delTTAG microdeletion in exon 27, whereas another patient had the previously reported c.1705 + 1G>T mutation in the splice donor sequence of intron 17, which activated a cryptic splice site (Schimpf *et al.*, 2006). The other four patients harboured three new mutations, inducing either splice defects (c.1516 + 1G>C in intron 15, one patient; c.2819-2A>C in intron 27, two patients) or a translational frame shift (c.1346_1347insC in exon 14, one patient). All the mutations are predicted to generate a truncated OPA1 protein as confirmed by cDNA analysis with total RNA isolated from patients' blood. All mutations were heterozygous and strictly co-segregated with individuals affected by optic atrophy in families with autosomal dominant inheritance.

Figure 1B shows the expression level of OPA1, mitofusin-1 (MFN1) and dynamin-related protein-1 (DRP1), the

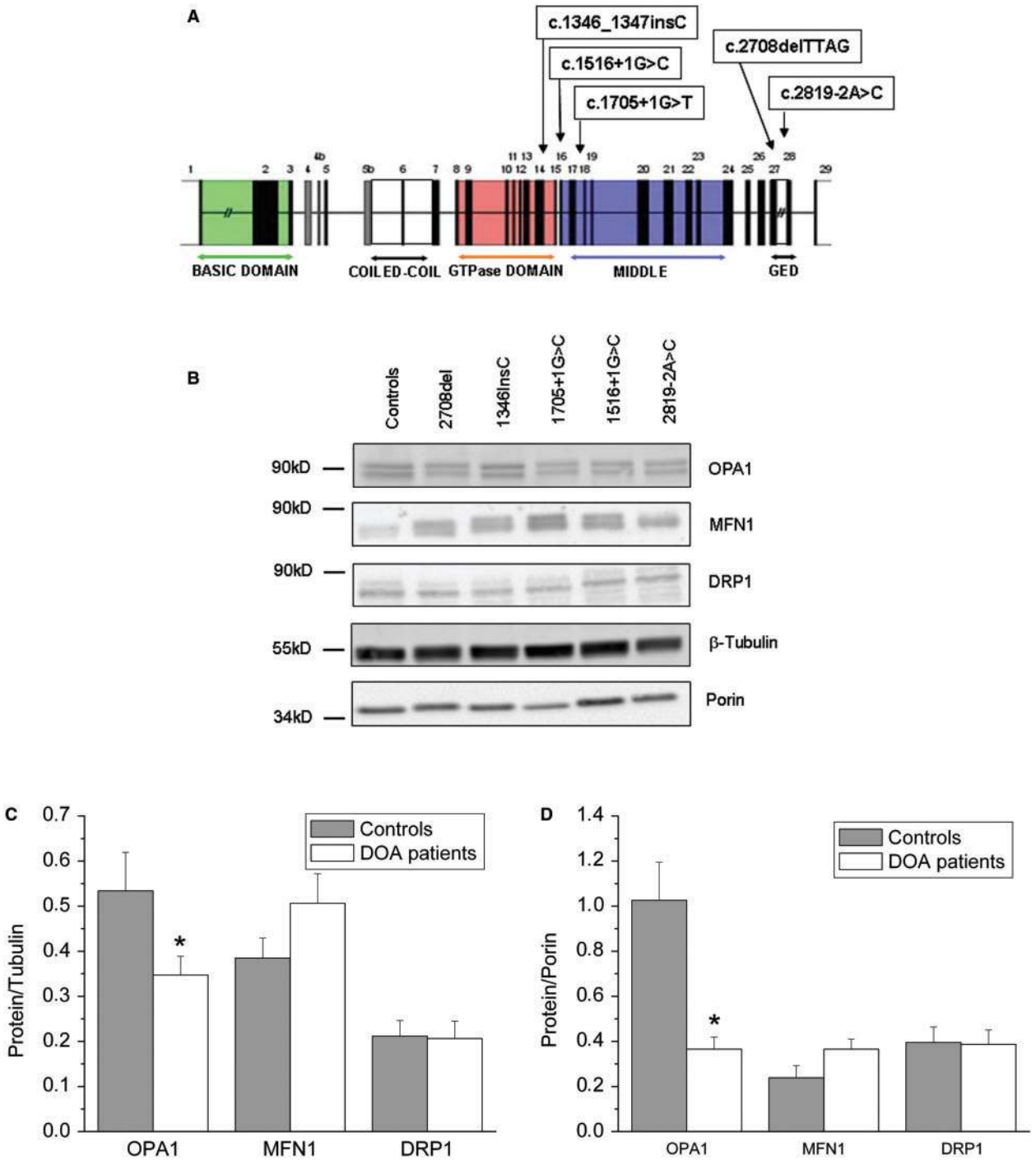

Fig. 1 Expression level of OPAI, mitofusin-1 and DRPI proteins in control and DOA fibroblasts. (**A**) Map of the *OPAI* gene and localization of the mutations analysed in this study. (**B**) Representative western blot of OPAI, MFNI, DRPI, β-tubulin and porin, carried out in fibroblast lysates obtained from one control and from patients carrying the indicated *OPAI* mutations. OPAI, MFNI and DRPI bands were normalized to β-tubulin (**C**) and porin (**D**) band density. Results are means ± SEM of four controls and eight DOA fibroblasts lysates obtained from three independent experiments and resolved in at least three blots.

main proteins involved in the processes of mitochondrial fusion and fission, determined in fibroblast lysates by western blotting. We detected two bands corresponding to OPA1, slightly above and below 90 kDa, likely corresponding to the 92 kDa and 86 kDa OPA1 isoforms previously reported in heart and brain. This pattern is similar to that shown by others using homemade polyclonal antibodies in mitochondria isolated from other tissues or in other cell types (Olichon et al., 2002). Two bands were also apparent for mitofusin-1. β-Tubulin and the mitochondrial

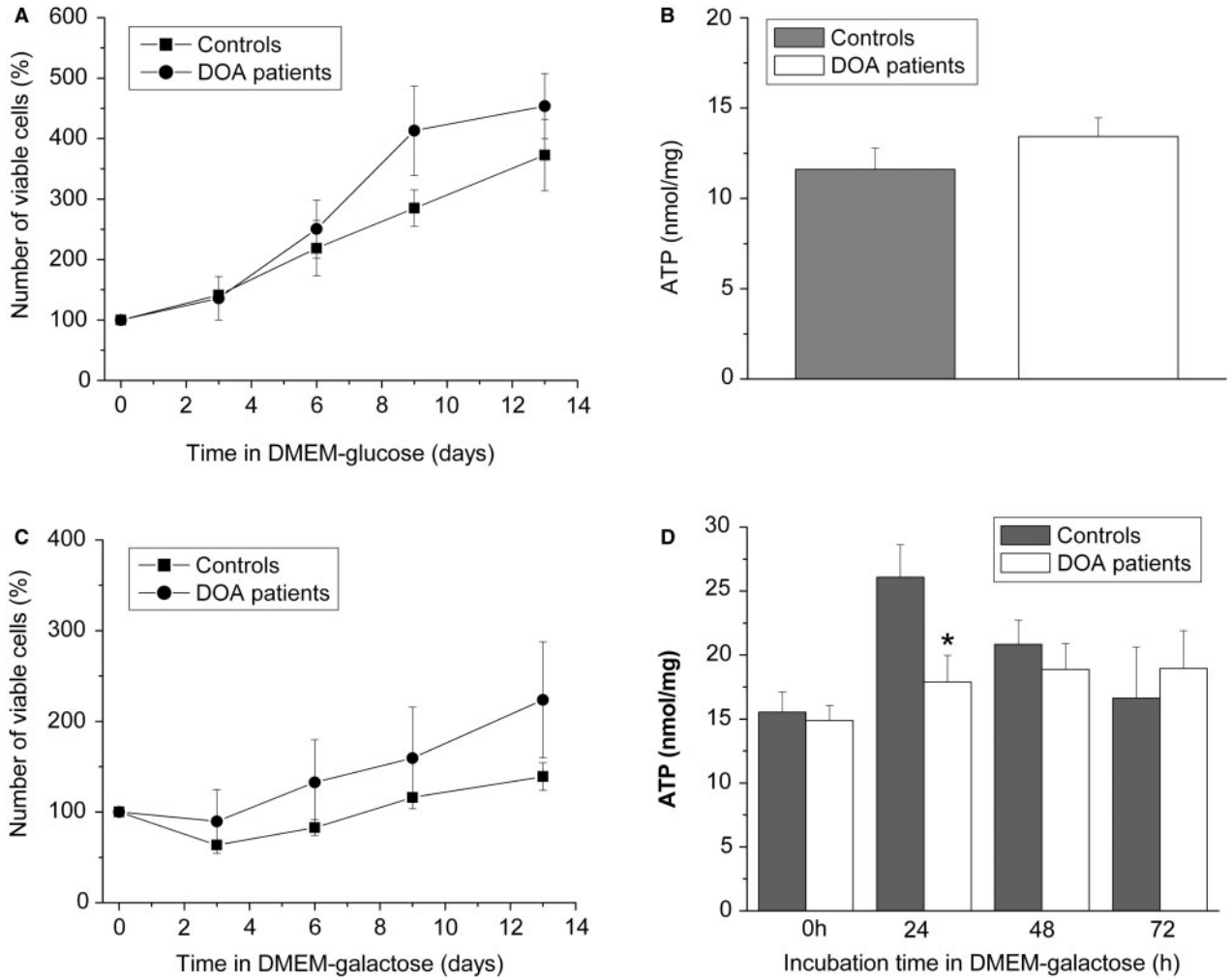

Fig. 2 Cell viability and ATP content of control and DOA fibroblasts. (**A**) Controls and DOA fibroblasts were incubated in DMEM-glucose medium for the times indicated. The MTT absorbance value at time zero was considered the 100% value of the number of viable cells. Each data point represents the mean ± SEM of values obtained from two controls and four DOA fibroblasts. Each cell line was tested at least in triplicate. (**B**) The ATP content of five controls and eight DOA fibroblasts in DMEM-glucose medium was determined in at least three different preparations for each cell line. (**C**) Controls and DOA fibroblasts were incubated in DMEM-galactose medium for the times indicated and cell viability determined. The 100% value is the MTT absorbance value determined in DMEM-glucose (time = 0). Each data point represents the means ± SEM of values obtained from two controls and four DOA fibroblasts, each tested in three to five independent experiments. (**D**) ATP levels of controls and DOA fibroblasts were determined at different times of incubation in galactose medium and expressed as nanomoles per milligram protein. Data are means ± SEM of values obtained from three controls and seven DOA fibroblasts, each tested in three to five independent experiments. Asterisk denotes a value significantly different from that of controls at the same time ($P < 0.05$).

protein porin were used as controls for quantification. Normalization relative to both β-tubulin and porin showed a significant reduction of OPA1 protein in DOA fibroblasts compared to controls (Fig. 1C and D), confirming that haploinsufficiency results from mutations predicted to generate a truncated protein. Conversely, mitofusin-1 levels were slightly upregulated in DOA fibroblasts, this being more evident when normalized to β-tubulin compared to porin. DRP1 on the other hand remained unchanged in both cases (Fig. 1C and D).

The growth capability and ATP content of control and DOA fibroblasts bearing *OPA1* mutations were not significantly different in glucose medium (Fig. 2A and B). To further characterize the energetic competence of DOA cells, we assessed their viability during incubation in a glucose-free medium containing galactose. Under these conditions, cells are forced to rely predominantly on oxidative phosphorylation for ATP synthesis, given the low efficiency of this carbon source to feed the glycolytic pathway (Robinson *et al.*, 1992). Growth in galactose medium was significantly slower than in glucose medium for both DOA and control cells. Again, in galactose medium no significant difference was observed between controls and DOA patients. Under both growth conditions, the number of DOA fibroblasts was higher at all times compared to controls although not significantly different

and within the range of variation previously experienced by similar cell growth experiments in our laboratory (Figure 2A and C). Furthermore, the ATP levels of both control and DOA fibroblasts increased after 24 h of incubation in galactose medium compared to glucose medium, as a consequence of the shift from glycolytic to oxidative metabolism. However, this ATP increase was significantly higher in controls compared to patient fibroblasts at 24 h, this difference being negligible after 48 and 72 h of incubation (Fig. 2D). Therefore, DOA fibroblasts initially showed a lower capacity to produce ATP when forced to utilize solely the respiratory chain for their energy production. However, at longer incubation times their ATP levels were comparable to those displayed by control cells and they were viable and able to grow in galactose medium.

Mitochondrial network of DOA fibroblasts

Considering that OPA1 function is thought to be relevant in mitochondrial network organization, we investigated the mitochondrial morphology of DOA fibroblasts bearing the *OPA1* microdeletion in glucose and after 24 h incubation in galactose medium. After loading with Mitotracker Red and examination by fluorescence microscopy, fibroblasts could be scored into three categories on the basis of mitochondrial morphology. Class I cells showed a typical filamentous network, class II cells showed filamentous mitochondria containing balloon-like structures and class III cells showed complete fragmentation resulting in only isolated mitochondrial balloons. Representative images of these three classes of mitochondrial morphology are shown in Fig. 3A–C.

In glucose medium, both control and DOA fibroblasts exhibited a similar percentage of class I and class II cells (Fig. 3D). After 24 h incubation in galactose medium, control fibroblasts maintained the same distribution of the three cell classes. Conversely, in DOA fibroblasts the percentage of class I cells decreased, whereas that of class II and III consistently increased, these values becoming significantly different from controls (Fig. 3E). Fragmentation of the mitochondrial network has frequently been reported in cells undergoing apoptosis (Youle and Karbowski, 2005). However, the nuclear morphology, as evaluated after Hoechst staining, in all three classes of mitochondrial network organization never displayed chromatin condensation (insets of Fig. 3A–C), clearly indicating that despite the different degrees of mitochondrial fragmentation these cells did not spontaneously undergo apoptosis.

Representative images of the mitochondrial morphology of control and DOA fibroblasts with the other mutations in DMEM-glucose and DMEM-galactose medium are shown in Fig. 4. Also in fibroblasts bearing these mutations, the percentage of class II and III consistently increased in galactose medium. It is therefore apparent that although DOA fibroblasts are still able to maintain ATP levels and growth capability in galactose medium, a large percentage of cells undergo a drastic remodelling of the mitochondrial network when forced to utilize oxidative phosphorylation for ATP production.

Major disruption of the overall organization of the cristae has been reported in cells where OPA1 expression has been downregulated by RNA interference (Olichon *et al.*, 2003). Ultrastructural investigation by transmission electron microscopy was therefore carried out in fibroblast mitochondria under the two different growth conditions. In glucose medium, a remarkable decrease in the number and organization of cristae was evident in ~50% of DOA fibroblasts with the *OPA1* microdeletion compared with controls (Supplemental Fig. 1A and C). In the large majority of images control fibroblasts had a regular pattern of parallel organization of cristae along the short diameter (Supplemental Fig. 1A). Growth in galactose medium occasionally altered cristae organization also in controls compared to glucose medium, and further affected the DOA fibroblast mitochondria. In fact, aberrant elongation of isolated cristae running along the longitudinal diameter of the organelle was frequently observed, dramatically contrasting with the parallel organization essentially maintained in control mitochondria (Supplemental Fig. 1B and D).

Mitochondrial fusion in DOA fibroblasts with c.2708delTTAG microdeletion

The OPA1 protein has been implicated in the mitochondrial fusion process (Olichon *et al.*, 2003; Lee *et al.*, 2004; Chen *et al.*, 2005). A quantitative *in vivo* mitochondrial fusion assay, based on the measurement of the dilution rate of mito-PAGFP (Karbowski *et al.*, 2004), was used to evaluate whether this process was altered in DOA fibroblasts bearing the *OPA1* microdeletion. Small regions of cells transfected with mito-PAGFP were photoactivated and the decrease in fluorescence over time was determined by confocal microscopy. A representative image of one DOA fibroblast in glucose medium at 0, 30 and 60 min after photoactivation is shown in Fig. 5A. In glucose medium, the decrease in fluorescence intensity within the activated regions of DOA fibroblasts was significantly faster than in controls (Fig. 5C). After 24 h incubation in galactose medium, DOA fibroblasts presented both filamentous and balloon-like patterns of mitochondrial network. An example of the latter is shown in Fig. 5B. No class III cells with fragmented mitochondrial network were detected, possibly because these fibroblasts may be less susceptible to successful transfection with mito-PAGFP. The overall rate of mitochondrial fusion in galactose medium was similar in control and DOA cells (Fig. 5D). However, once we scored the DOA fibroblasts analysed in Fig. 5D according to mitochondrial morphology, about 40% of them belonged to class I and 60% to class II (Fig. 5E). When the decrease of mito-PAGFP fluorescence was re-calculated in the two different DOA cell populations

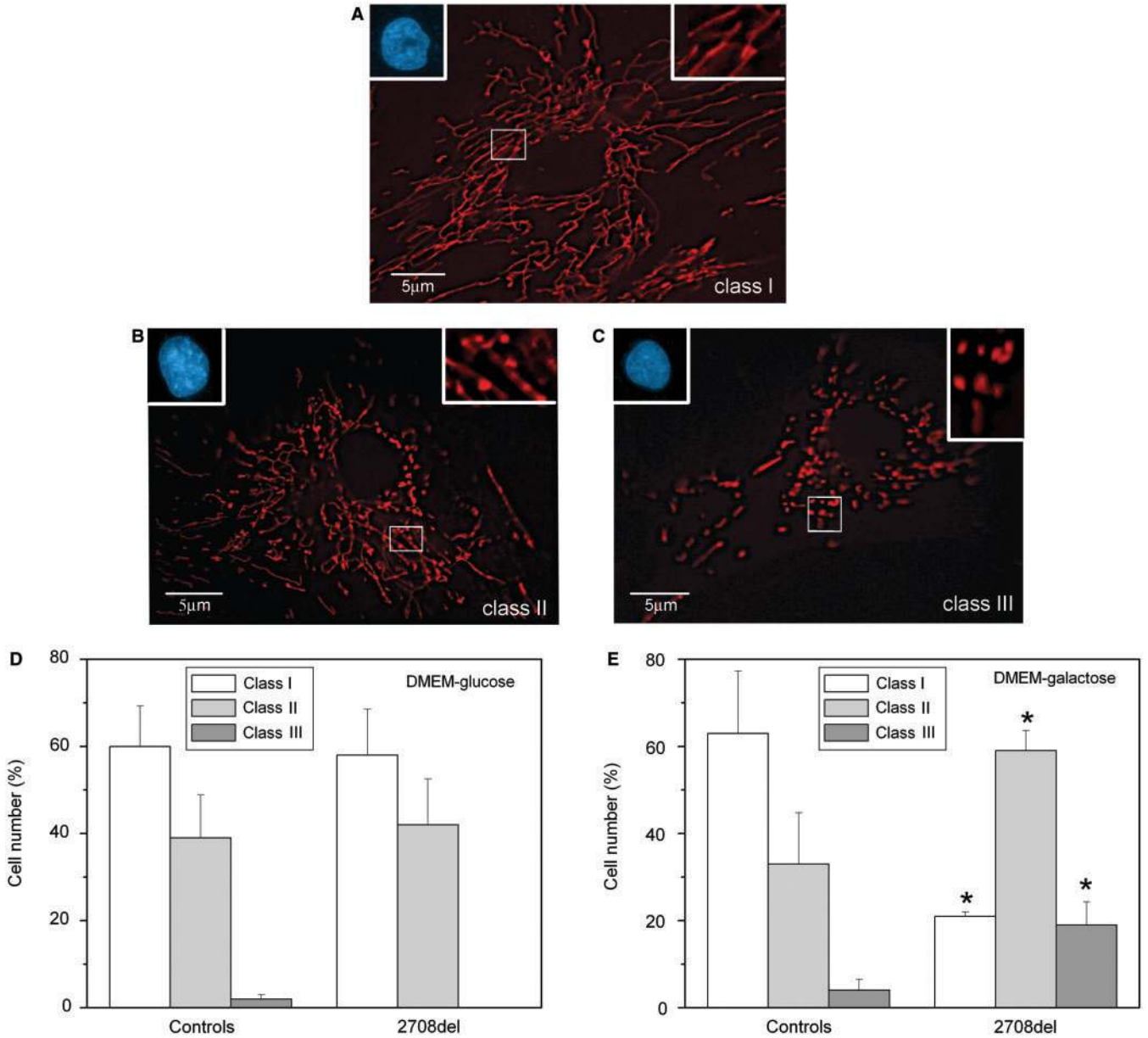

Fig. 3 Mitochondrial morphology. Control and DOA fibroblasts with the *OPA1* microdeletion were incubated in DMEM-glucose or in DMEM-galactose medium for 24 h, and then loaded with Mitotracker Red and Hoechst, as described in Materials and Methods section. Representative images of the three mitochondrial morphologies of DOA fibroblasts incubated in DMEM-galactose medium are shown: (**A**) class I; (**B**) class II; (**C**) class III. The inset at the right of each panel shows an enlarged detail of the mitochondrial network. The inset at the left shows the corresponding nuclear morphology. (**D, E**) Bar graphs show quantification of the three categories by blind test. Fifty-one control and 56 DOA fibroblasts were counted in glucose medium; 40 control and 44 DOA fibroblasts in galactose medium. Fibroblasts analysed were from three controls and three DOA patients. Asterisk denotes values significantly different from controls ($P < 0.01$).

(class I versus class II), it was apparent that mitochondrial fusion was almost abolished in class II cells, whereas in class I cells it remained faster than controls, similar to what was observed in glucose medium (Fig. 5F).

Mitochondrial ATP synthesis in fibroblasts with *OPA1* mutations

The lower capacity to produce ATP and the induction of a fragmented mitochondrial network under conditions of forced oxidative metabolism in galactose medium, in addition to the abnormal mitochondrial ultrastructure, prompted us to investigate the energetic efficiency of mitochondria in more detail. We measured the rate of ATP synthesis in digitonin-permeabilized cells, after normalization for the citrate synthase activity, an indicator widely used to evaluate mitochondrial mass. The values of citrate synthase activity of control and DOA fibroblasts were 132 ± 57 and 122 ± 50 nmol/min/mg, respectively in glucose medium and 124 ± 42 and 148 ± 61 nmol/min/mg,

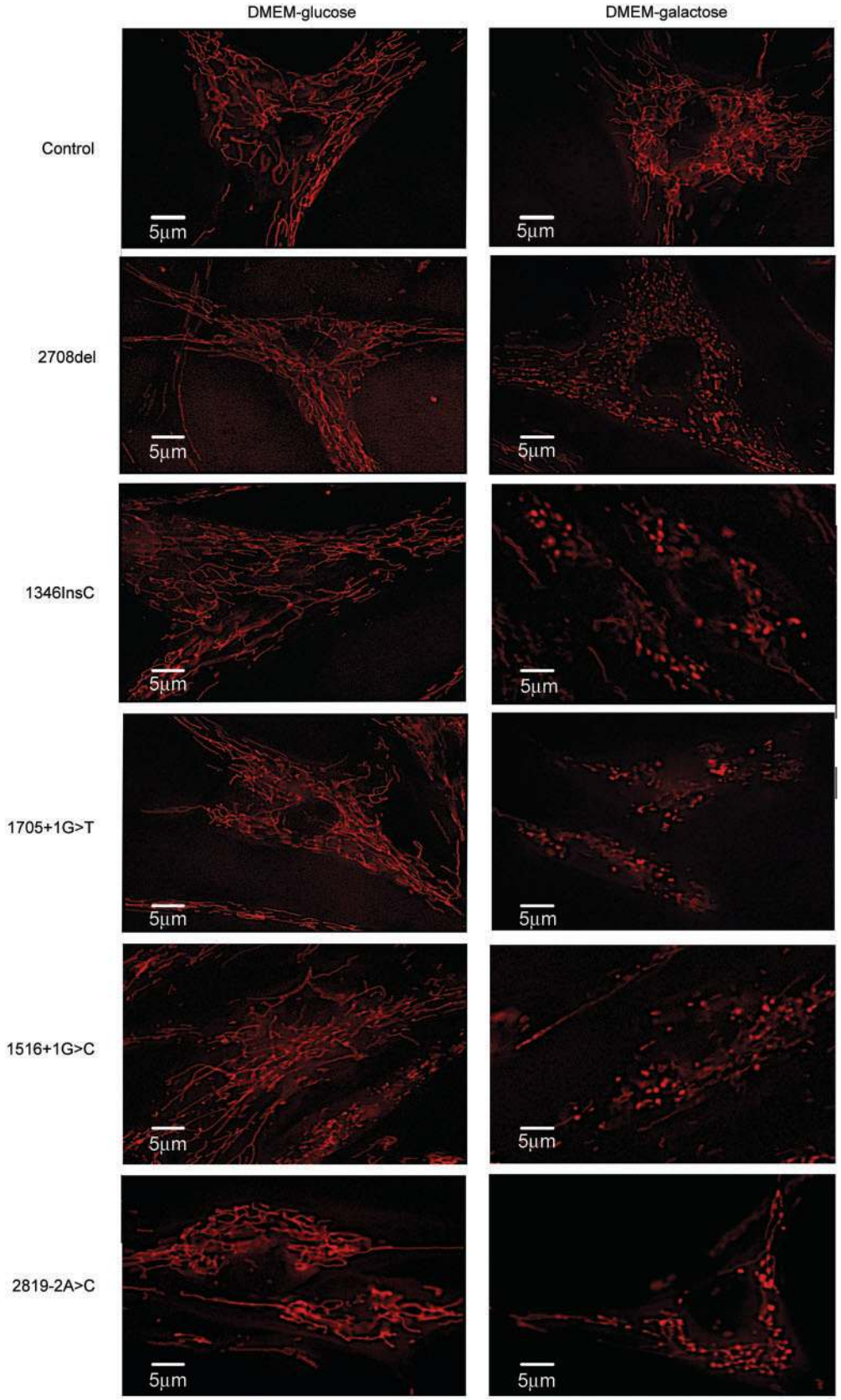

Fig. 4 Mitochondrial morphology of DOA fibroblasts with other *OPA1* mutations. DOA fibroblasts with the indicated *OPA1* mutations were incubated in DMEM-glucose or in DMEM-galactose medium for 24 h, and then loaded with Mitotracker Red as described in Materials and Methods section. Representatives out of eight similar images are shown for each condition.

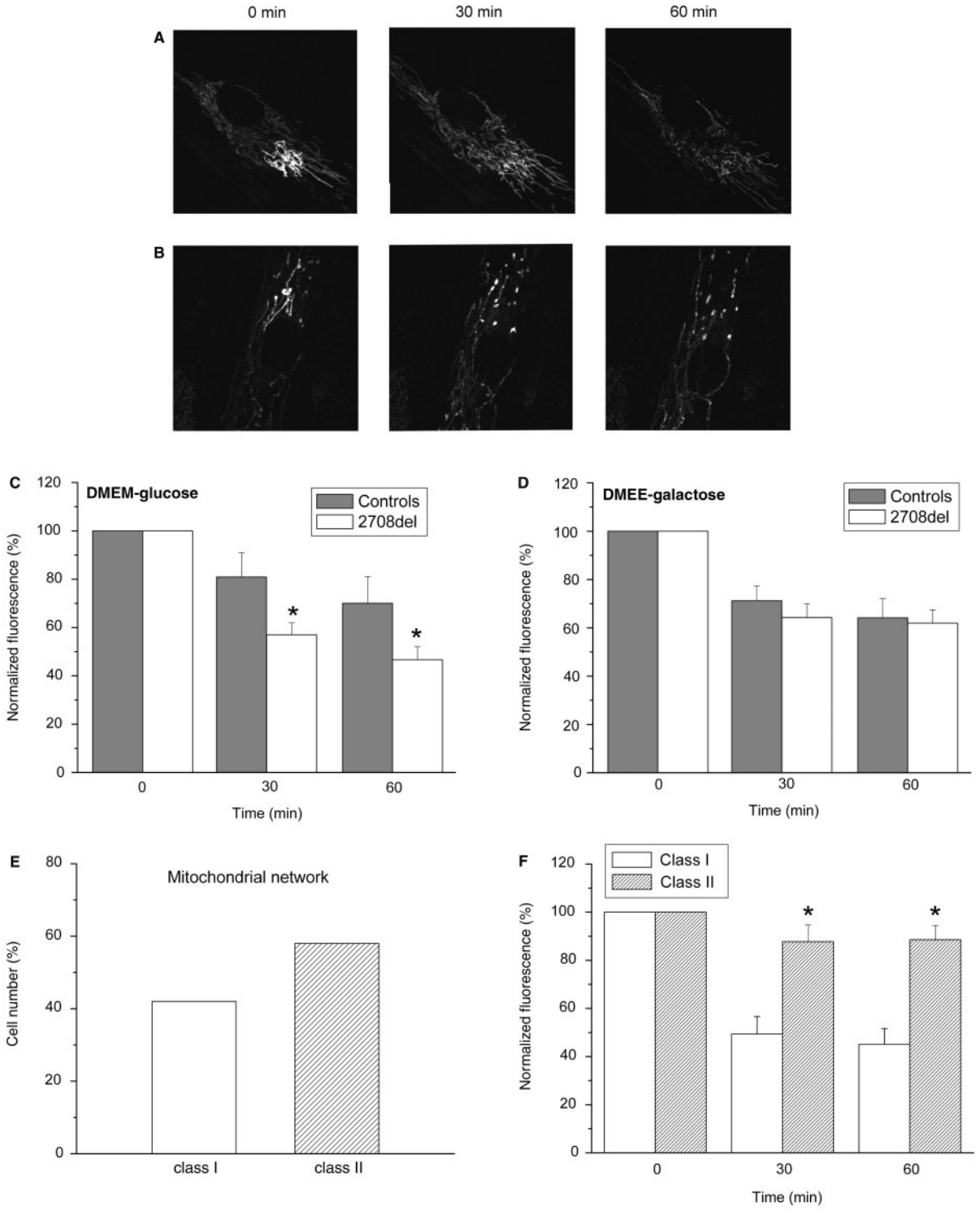

Fig. 5 Visualization and quantification of mitochondrial fusion in control and DOA fibroblasts with the *OPA1* mutation c.2708delTTAG. Control and DOA fibroblasts with the *OPA1* microdeletion were transfected with mito-PAGFP and observed using a confocal microscope. Representative images of one DOA fibroblast incubated in DMEM-glucose (**A**) or after 24 h incubation in DMEM-galactose medium (**B**) at 0, 30 and 60 min are shown. The values of mito-PAGFP fluorescence after 30 and 60 min were expressed as per cent of the fluorescence value at 0 min (100% value) in control and DOA fibroblasts incubated in DMEM-glucose (**C**) or DMEM-galactose (**D**). Data are the means ± SEM of control ($n = 45$) and DOA ($n = 50$) fibroblasts analysed. Fibroblasts were from two controls and two DOA patients. Asterisk denotes values significantly different from controls ($P < 0.01$). (**E**) The images of DOA fibroblasts incubated in DMEM-galactose medium analysed in panel D were scored into class I and class II categories. (**F**) The values of mito-PAGFP fluorescence of 50 DOA fibroblasts incubated in DMEM-galactose were grouped according to the mitochondrial morphology (class I versus class II). Asterisk denotes values significantly different between class I and class II cells ($P < 0.01$).

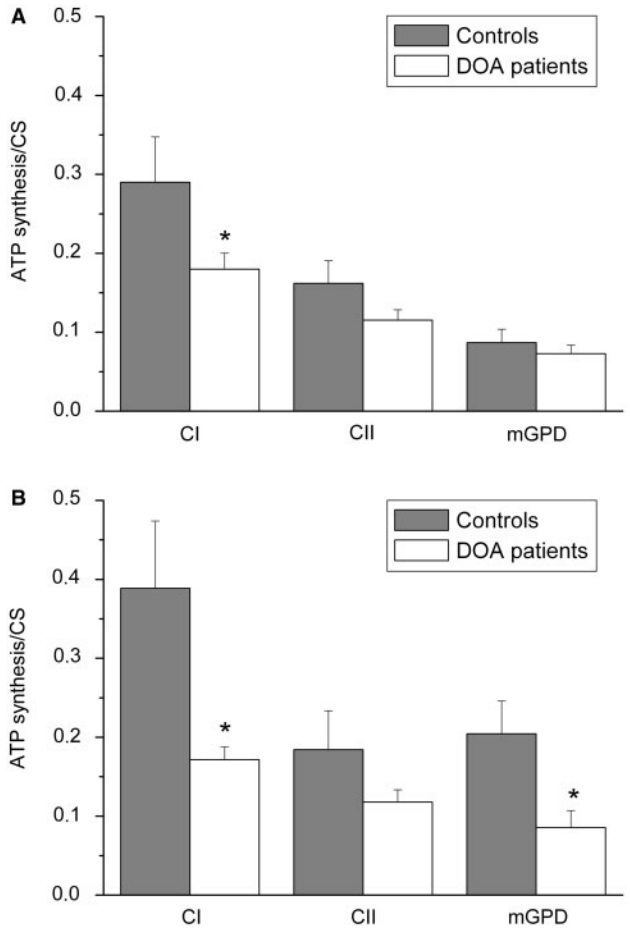

Fig. 6 Mitochondrial ATP synthesis in control and DOA fibroblasts. Fibroblasts incubated for 24 h in DMEM-glucose (**A**) or DMEM-galactose (**B**) were treated with 50 μg/ml digitonin and the rate of ATP synthesis driven by 5 mM pyruvate plus 5 mM malate (complex I) or 10 mM succinate plus 4 μM rotenone (complex II) or 25 mM glycerol 3-phosphate plus 4 μM rotenone (mGPD) was subsequently determined. The rate of ATP synthesis was normalized for citrate synthase (CS) activity. Data (mean ± SEM) were obtained in fibroblasts from five controls and seven DOA patients. The experiment was performed at least in duplicate. Asterisk denotes values significantly different from controls ($P < 0.05$).

respectively in galactose medium. As reported in Fig. 6A, in glucose medium the rate of ATP synthesis driven by the complex I substrates (pyruvate and malate) was significantly decreased in fibroblasts with *OPA1* mutations compared to controls. To evaluate the ATP synthesis excluding complex I, we used substrates transferring reducing equivalents into the electron transport chain to ubiquinone through complex II (succinate) or through the mitochondrial glycerol 3-phosphate dehydrogenase (mGPD). A tendency towards reduction, without reaching a statistical significance, was observed for complex II, whereas values similar to controls were obtained for mGPD (Fig. 6A).

After 24 h of incubation in galactose medium, in control fibroblasts the rates of mitochondrial ATP synthesis driven through complex I and mGPD, but not through complex II were increased compared to those in glucose medium, without reaching statistical significance (Fig. 6A and B). Conversely, in DOA fibroblasts ATP synthesis through all complexes was similar to that in glucose medium. Thus, in galactose medium ATP synthesis driven by complex I and also by mGPD was significantly different between DOA and control fibroblasts (Fig. 6B).

Overall, these results reveal a clearly defective oxidative phosphorylation prevalently through complex I, as a common pathological feature characterizing all the *OPA1* mutations investigated in this study.

Analysis of mtDNA content and respiratory chain complexes in DOA fibroblasts

A reduced mtDNA copy number has been reported in leucocytes from DOA patients bearing different *OPA1* mutations (Kim *et al.*, 2005), thus providing a potential link between *OPA1* mutations and the respiratory chain defect. However, determination of the mtDNA content by quantitative real-time PCR showed an increase in mtDNA copy number per cell in DOA fibroblasts compared with controls, which was significant in DMEM-glucose medium, but not in galactose medium (Fig. 7A).

Impairment of oxidative phosphorylation could reflect a defective assembly or a decreased number of respiratory complexes. To investigate respiratory complex assembly, mitochondria were isolated from fibroblasts derived from one control and three DOA patients and respiratory complexes were resolved by blue native electrophoresis (Nijtmans *et al.*, 2002). Bands corresponding to complexes I, II, III, IV and V were consistently well resolved. No significant difference was observed between control and DOA patients (Supplemental Fig. 2). Furthermore, the expression level of NDUFA9, ND6 and NDUFB6 subunits of complex I was also determined in the mitochondrial fractions (Fig. 7B). Normalization to porin showed that the levels of these complex I subunits were slightly increased in DOA fibroblasts, this effect being greater, but not significant, for the ND6 subunit (Fig. 7C). Similarly, the level of the complex II FP subunit was not affected (data not shown).

OPA1 directly interacts with respiratory complexes and with AIF

To explore the hypothesis that the OPA1 protein could influence oxidative phosphorylation through a physical interaction with one or more of the respiratory complexes, cellular lysates from controls and DOA fibroblasts bearing four different *OPA1* mutations were immuno-precipitated with anti-OPA1 antibody and immunoblotted with antibodies specific to individual structural subunits of the respiratory complexes. Figure 8A shows that the 39-kDa

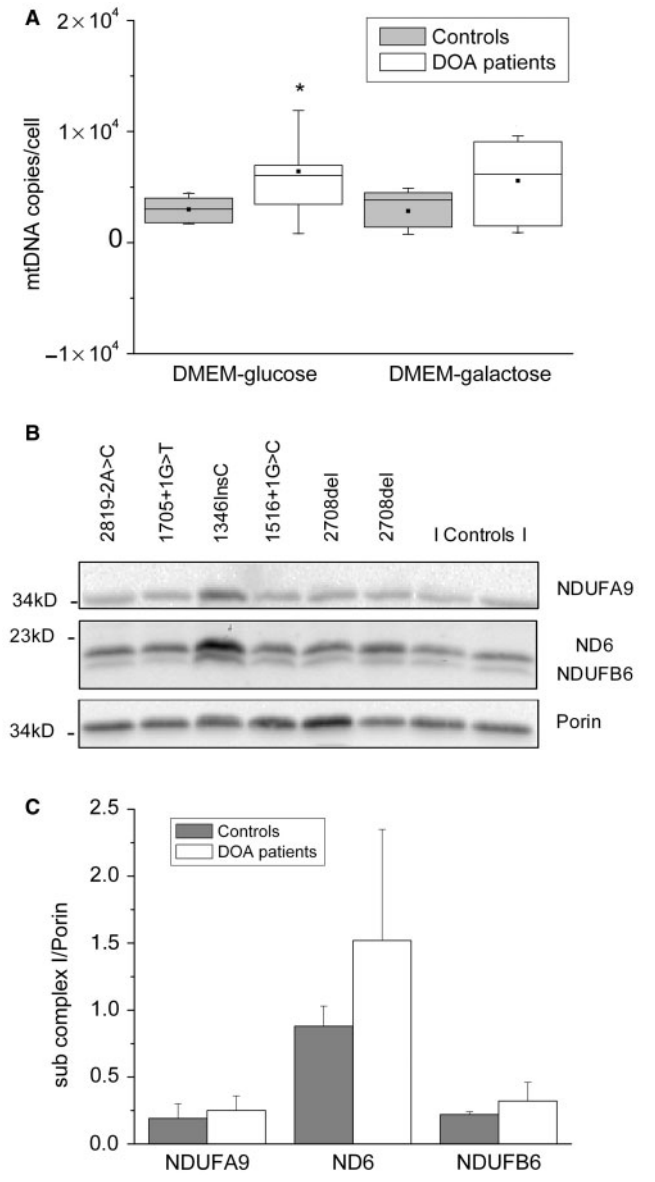

Fig. 7 Determination of mtDNA copy number and expression level of complex I subunits in control and DOA fibroblasts. (**A**) Fibroblasts from controls and DOA patients were incubated in DMEM-glucose medium or for 24 h in DMEM-galactose medium and mtDNA copies/cell calculated for each sample from the ratio between mtDNA copies and nDNA copies multiplied by two. Data were obtained in fibroblasts derived from four controls and six DOA patients, each tested in at least two experiments run in triplicate. Comparative box plots are shown: the top and bottom of the box indicate the 25th and 75th percentiles, the middle line indicates the median and the black square shows the mean numbers measured in each group. The whiskers indicate the 5th and 95th percentiles. Asterisk denotes values significantly different from controls ($P < 0.05$) determined by the Mann–Whitney Rank Sum Test. (**B**) The expression level of NDUFA9 (39 kDa), ND6 (20 kDa) and NDUFB6 (17 kDa) subunits of complex I and of porin was determined in mitochondria isolated from control and DOA fibroblasts by western blot. A representative out of two similar blots is shown. (**C**) Each band was normalized to porin band density. Results are means ± SEM ($n = 4$ controls; $n = 12$ DOA).

(NDUFA9) subunit of complex I, the 70-kDa (FP) subunit of complex II and the core II subunit of complex III co-precipitated with OPA1, whereas subunit I of complex IV was not detected. It is worth noting that similar results were obtained by co-immunoprecipitation experiments using both cellular lysates or mitochondrial fractions (data not shown).

Given that AIF has been shown to participate in complex I assembly and maintenance (Vahsen *et al.*, 2004), the same nitrocellulose membranes were also immunoblotted with anti-AIF antibody revealing a high affinity interaction between OPA1 and AIF. Similar results were obtained when cellular lysates were immunoprecipitated with anti-AIF antibody (Fig. 8B). Furthermore, when we tested the same nitrocellulose membranes with antibodies against actin, tubulin and DRP1 we did not detect any signal (data not shown), suggesting that the interaction among OPA1, AIF and respiratory complexes I, II and III was specific.

We then used anti-OPA1 and anti-AIF antibodies for immunoprecipitation of cellular lysates obtained from the mtDNA-lacking 143B206 Rho0 cells and the original parental osteosarcoma-derived 143B.TK$^-$ cells (King and Attardi, 1989). The 143B206 Rho0 cells completely lack the mitochondrial genome and consequently do not have a functional respiratory chain. It has been shown that due to the absence of the mtDNA-encoded ND subunits the complex I is only partially assembled (Ugalde *et al.*, 2004). Consistently with this notion, Fig. 8C (input) shows that 143B206 Rho0 cells expressed drastically reduced levels of the nuclear encoded NDUFA9 subunit of complex I compared to the parental 143B.TK$^-$ cells, as previously reported (Ugalde *et al.*, 2004). Accordingly, NDUFA9 subunit was not detected in the anti-OPA1 and anti-AIF immunoprecipitates. Conversely, under these conditions of partially assembled complex I, the cross-immunoreactivity between OPA1 and AIF was maintained in 143B206 Rho0 cells, similar to the parental 143B.TK$^-$ cells (Fig. 8C).

Sensitivity of DOA fibroblasts to a pro-oxidant agent

OPA1 mutations have been shown to sensitize fibroblasts to apoptotic cell death induced by staurosporine (Olichon *et al.*, 2007*b*). Figure 9A shows that incubation with the pro-oxidant agent t-BH induced a significantly more rapid loss of viability in DOA fibroblasts compared to controls. This was associated with a marked decrease of ATP content, which became significant after 16 h (Fig. 9B). Analysis of nuclear morphology showed that the number of nuclei exhibiting chromatin condensation was significantly increased in DOA fibroblasts treated with t-BH compared to controls (71 ± 5%, $n = 50$ in DOA and 29 ± 9%, $n = 46$ in controls). Representative images of nuclei before and after t-BH treatment are reported in Fig. 9C and D.

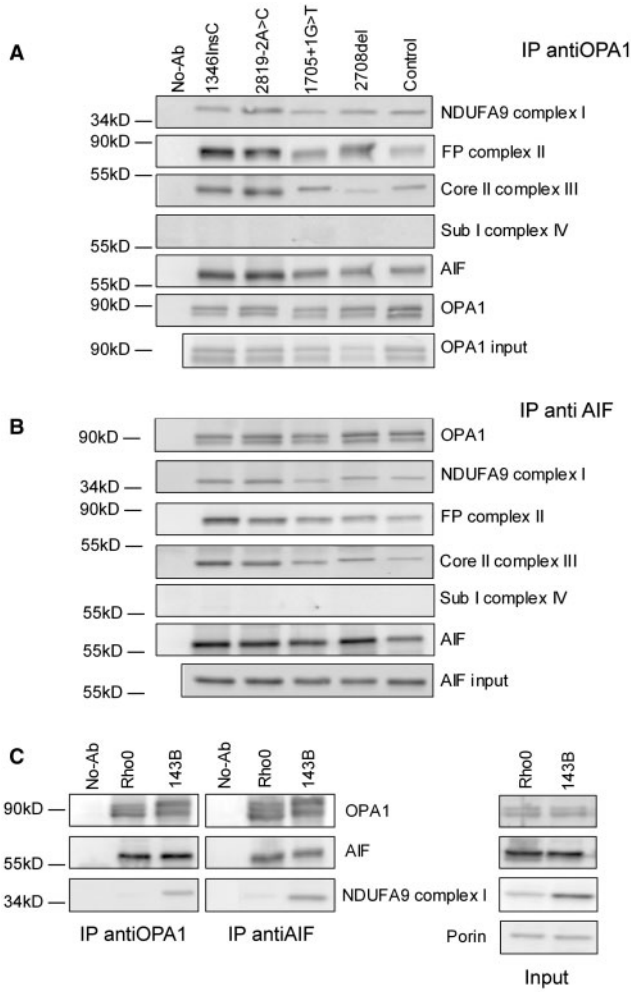

Fig. 8 Interaction of OPA1 with mitochondrial proteins. (**A**) Cellular lysates obtained from control and DOA fibroblasts with the indicated *OPA1* mutations were immunoprecipitated with anti-OPA1 antibody and immunoblotted with antibodies against the NDUFA9 subunit of complex I, the FP subunit of complex II, the core II subunits of complex III, the subunit I of complex IV, AIF and OPA1. The reaction mixture prior to immunoprecipitation was also analysed by immunoblotting using anti-OPA1 antibody (input). In each blot, immunoreactivity between lysates and protein-A Sepharose in the absence of antibodies was determined (no-Ab). (**B**) The same lysates tested in panel (A) were immunoprecipitated with antibody against anti-AIF and revealed with the same antibodies used in panel (A). (**C**) Cellular lysates obtained from 143B206 Rho0 and 143B.TK$^-$ cells were immunoprecipitated with anti-AIF or anti-OPA1 antibodies and immunoblotted with antibodies against OPA1, AIF and the NDUFA9 subunit of complex I. The reaction mixture prior to immunoprecipitation was analysed by immunoblotting using anti-OPA1, AIF, NDUFA9 and porin antibodies (input). Blots are representative of three similar experiments.

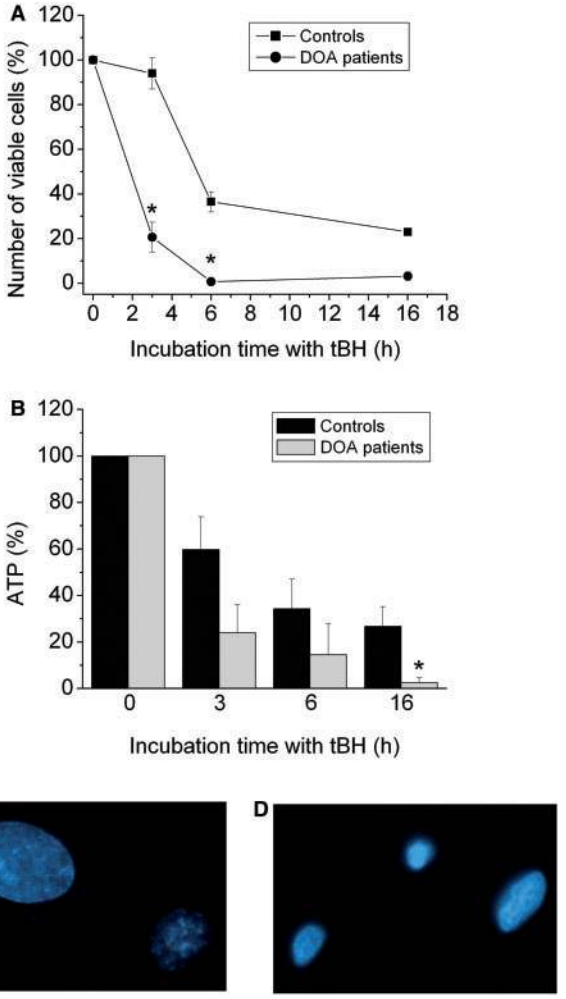

Fig. 9 Viability and ATP content of control and DOA fibroblasts treated with t-BH. Control and DOA fibroblasts were incubated with 250 μM t-BH for the times indicated and the number of viable cells (**A**) and the ATP content (**B**) were determined as described in Fig. 2. Data are expressed as % of the values measured in DMEM-glucose before addition of t-BH (time = 0). Data are means ± SEM of values obtained from two controls and two DOA fibroblasts, each tested in at least three independent experiments. Asterisk denotes a value significantly different from those of controls at the same time ($P < 0.05$). Representative images of Hoechst-loaded nuclei from one DOA patient before (**C**) and after 6 h incubation with t-BH (**D**).

Discussion

The present study shows that the common c.2708delTTAG *OPA1* microdeletion and four other pathogenic mutations, all predicted to generate a truncated protein, cause a significant reduction in the level of the OPA1 protein in fibroblasts. This would support the hypothesis that the pathological mechanism involves haploinsufficiency. Reduced OPA1 expression was associated with a significant impairment of oxidative phosphorylation, mostly mediated at the level of complex I. When cells were forced to use oxidative metabolism in galactose medium, ATP levels failed to increase as in controls, but cells remained viable for several days. Furthermore, growth in galactose medium strongly promoted an extensive mitochondrial network remodelling and inhibited mitochondrial fusion in a consistent subset of cells. We also documented that OPA1 mutant fibroblasts were more prone to cell death than controls after an exogenous oxidative stress. Finally, we

showed for the first time that OPA1 interacts with some respiratory complexes and AIF.

Some indications that defective oxidative phosphorylation is caused by *OPA1* mutations have been previously reported. A reduction of mitochondrial ATP synthesis through the respiratory chain as a whole was shown in fibroblasts from patients suffering from DOA and sensorineural deafness patients carrying the severe mis-sense *OPA1* mutation R445H (Amati-Bonneau *et al.*, 2005), which is not predicted to generate a truncated protein. We also reported that the very same patients bearing the c.2708delTTAG microdeletion in the *OPA1* gene, whose cell lines were investigated in this study, had a defective oxidative phosphorylation in skeletal muscle as detected by phosphorus MR spectroscopy (Lodi *et al.*, 2004). The present study in fibroblasts from these same patients, pooled with others bearing four different pathogenic mutations, shows for the first time that the rate of mitochondrial ATP synthesis was significantly reduced at the level of complex I, with this phenomenon being more evident in galactose medium. The investigation of ATP synthesis driven by complex II and mGPD did not reveal any other major site of impairment in DOA fibroblasts, thus pointing to complex I as the candidate for the defective oxidative phosphorylation. The failure to increase ATP levels after 24 h of incubation in galactose medium, shown by DOA cells compared to controls, was paralleled by the significant difference in complex I and mGPD-driven ATP synthesis seen between controls and DOA fibroblasts in the same conditions. The observed upregulation of electron flux through complex I and mGPD in control cells when forced to use mitochondrial oxidative phosphorylation to sustain ATP production deserves further study, as it seems to be an interesting compensatory mechanism, and one which DOA cells failed to operate. Overall, these data suggest that a respiratory chain impairment is common to these *OPA1* mutations, and complex I seems to play a major role. However, it is noteworthy that under forced oxidative metabolism in galactose medium the viability of all *OPA1* mutant fibroblasts was essentially preserved, indicating that a sufficient ATP production is maintained in DOA.

Why ATP synthesis is impaired prevalently through complex I needs to be explained. Complex I is the largest complex of the respiratory chain and the first site for electron transfer and energy conservation in oxidative phosphorylation (Brandt, 2006). It is built up of 46 subunits in mammals, seven of which are encoded by mtDNA. The gene expression of nuclear and mitochondrial-encoded subunits of complex I, and their coordinated assembly in human cells are both still poorly understood processes (Ugalde *et al.*, 2004). Furthermore, only a few proteins directly interacting with complex I and possibly involved in its assembly and stabilization have been identified, such as AIF, B17.2L, NDUFAF1 and possibly paraplegin (Atorino *et al.*, 2003; Vahsen *et al.*, 2004; Ogilvie *et al.*, 2005; Vogel *et al.*, 2005).

Kim and colleagues recently reported a small reduction of mtDNA copy number in leucocytes from DOA patients bearing different *OPA1* mutations (Kim *et al.*, 2005). Both mtDNA and OPA1 protein are anchored to the inner mitochondrial membrane and it was reasoned that the destabilization of cristae organization induced by *OPA1* mutations, as was also shown by our ultrastructural findings, may disrupt the stability of mtDNA nucleoids leading to a partial depletion. This would provide a potential link between *OPA1* mutations and the respiratory chain defect. Furthermore, considering that complex I is over-represented in terms of structural genes encoded by mtDNA (seven ND subunit genes), it is reasonable to speculate that partial mtDNA depletion may first and prevalently impair complex I function. However, this hypothesis was not confirmed by our evaluation of mtDNA copy number in DOA fibroblasts where, contrary to expectations, we observed a significant increase in mtDNA content. This may be interpreted as a classical compensatory mechanism for an oxidative phosphorylation defect, as commonly seen in patients with mitochondrial encephalomyopathies (DiMauro and Schon, 2003). Furthermore, we observed no decrease in the expression levels of a few complex I (NDUFA9, NDUFB6 and ND6) and complex II (FP) subunits for any of the *OPA1* mutations investigated. The augmented levels of the ND6 subunit indicate an increase in mitochondrial biogenesis. The results of blue native electrophoresis further rule out the occurrence of a defective assembly of the respiratory complexes.

The immunoprecipitation experiments indicate for the first time that OPA1 and AIF physically interact, and that both proteins associate with subunits of the respiratory complexes. This interaction between OPA1 and AIF persisted even when the respiratory complexes containing mtDNA-encoded subunits were only partially assembled, in particular complex I, as shown by our experiments with the 143B206 Rho0 cells. However, from this set of experiments we did not detect differences between *OPA1* mutant and control fibroblasts. These results suggest that AIF and OPA1 may have a complex role in regulating and stabilizing the respiratory chain, possibly having a major impact on complex I. Both proteins are located in the same compartment, the inner mitochondrial membrane, which also hosts the respiratory chain complexes. There is accumulating evidence that both OPA1 and AIF have multifunctional roles. OPA1 has been shown to accomplish different unrelated functions in mitochondrial network dynamics and in regulating cristae organization, cytochrome c storage and apoptosis (Olichon *et al.*, 2003; Frezza *et al.*, 2006), and also in mtDNA stability (Amati-Bonneau *et al.*, 2007; Hudson *et al.*, 2007). AIF is a flavoprotein with an NADH oxidase activity, which has a further role in stabilizing complex I and, once released, becomes a pro-apoptotic factor (Vahsen *et al.*, 2004). We propose therefore a new scenario where the OPA1 protein may play a role in the respiratory chain by interacting with

other proteins such as AIF as shown here, and also paraplegin as recently reported (Ishihara *et al.*, 2006). Thus, OPA1 haploinsufficiency may lead to a defective oxidative phosphorylation as clearly identified in this and previous studies (Lodi *et al.*, 2004). Furthermore, a well-established propensity of OPA1 mutant cells to undergo apoptosis, which has been documented by others (Olichon *et al.*, 2007*b*) and also in this study, may well relate to the release of cytochrome c, as shown by Frezza and colleagues (2006), but also to differences in the availability of other pro-apoptotic factors, such as AIF.

The other set of results from this study concerns the mitochondrial morphology of fibroblasts carrying *OPA1* mutations. The morphology of mitochondria from patients was similar to that of control cells in glucose medium, whereas it changed remarkably, displaying fragmented/balloon-like mitochondria, when cells were forced to use oxidative metabolism in galactose medium. Our data regarding mitochondrial morphology are in agreement with the current concept that mutations inducing haploinsufficiency do not influence the mitochondrial network in glucose medium (Olichon *et al.*, 2006). We also provided the first quantitative evaluation of the fusion process in OPA1 mutant cells, closely associated with the mitochondrial network organization. DOA cells with balloon-like mitochondrial morphology essentially lacked fusion events, whereas unexpectedly, those with a filamentous mitochondrial network showed a significantly increased fusion rate. Our observation that mitofusin-1 levels were increased, albeit not significantly, may indicate a compensatory mechanism for OPA1 haploinsufficiency, possibly explaining the increased fusion rate in the subset of cells maintaining a filamentous mitochondrial network.

It is intriguing that when downregulated or mutated, both AIF and paraplegin have been linked to defective complex I and optic atrophy in animals and humans (Klein *et al.*, 2002; Atorino *et al.*, 2003). In fact, the Harlequin mouse with reduced AIF expression is characterized pathologically by an early and prevalent degeneration of RGCs leading to optic atrophy, and a defect in complex I stabilization (Ishihara *et al.*, 2006). Similarly, paraplegin mutations in humans lead to complicated spastic paraplegia, which includes optic atrophy, and again to a defective assembly of complex I (Atorino *et al.*, 2003). Likewise, these observations suggest that defective OPA1, AIF and paraplegin proteins share a final common pathological mechanism, which involves complex I impairment and leads to degeneration of RGCs and optic atrophy. However, most remarkably, the finding that complex I is impaired in DOA directly establishes a link with LHON, the other non-syndromic mitochondrial optic neuropathy sharing many features with DOA and caused by mtDNA point mutations affecting complex I (Carelli *et al.*, 2004, 2007). Both diseases share a selective loss of RGCs, preferentially hitting the small, less myelinated and more energy-dependent fibres of the papillomacular bundle. The main difference distinguishing DOA and LHON is the timing of the degenerative processes, which in most cases is acute/subacute in LHON with massive and synchronized loss of RGCs, and slowly progressive with frequent stable conditions in DOA. However, the clinical end-point of optic atrophy and severe visual impairment is identical. Our study strongly suggests the existence of common steps in the pathogenic mechanism in both DOA and LHON. In particular, the link between complex I dysfunction and mitochondrial network organization is of great interest in the context of mitochondrial biogenesis in RGC somata and mitochondrial axonal transport along the optic nerve (Hollenbeck and Saxton, 2005). It is known that a skewed distribution of mitochondria characterizes the unmyelinated initial portion of the RGC axons before the lamina cribrosa, where mitochondria are abundant, compared to the postlaminar optic nerve, which is myelinated and has less mitochondria (Carelli *et al.*, 2004, 2007). Thus, any perturbation of organellar transport in axons and mitochondrial distribution seems very relevant to the degenerative process of RGCs. The evidence that mitochondrial fusion is altered in DOA and the fact that this relates to an impairment prevalently expressed at complex I level, suggests that the complex I defect in LHON may have similar effects on mitochondrial network organization. The further and final link paralleling DOA and LHON is the evidence that in both disorders cells are predisposed to undergo apoptosis, under the appropriate triggering conditions (Danielson *et al.*, 2002; Ghelli *et al.*, 2003; Zanna *et al.*, 2005).

In conclusion, our study on fibroblasts with pathogenic mutations in the *OPA1* gene inducing haploinsufficiency suggests that there are different layers of interconnected consequences at the cellular level. First, we link the *OPA1* mutations to a mitochondrial respiratory chain dysfunction, which is mainly mediated by complex I, possibly through a direct interaction of the OPA1 protein with the respiratory complexes and other proteins such as AIF. We are well aware that this new scenario suggested by the current results warrants an extensive further set of investigations. Second, we show a close relationship between the energetic state of the cell and the mitochondrial network organization, emphasizing the central role of OPA1 in both functions. Thus, we propose that energy production to transport and distribute mitochondria within the axonal system in association with mitochondrial network dynamics must both be crucial to maintain the efficiency of this cellular system. When this fails, a propensity to apoptotic death of RGCs may occur leading to progressive neurodegeneration and optic atrophy.

Supplementary material

Supplementary material is available at *Brain* online.

Acknowledgements

We thank Dr A. Antignani, National Institutes of Health, Bethesda, for technical support with confocal microscopy and Dr A. Iuso, University of Bari, for help and suggestions for BN PAGE. We also thank Dr R. Liguori and Dr V. Donadio at the Department of Neurological Sciences for kindly performing the skin biopsies. C.Z. was a recipient of a Marco Polo Fellowship from the University of Bologna. This work was partially supported by grants from Ministero della Salute, progetto di ricerca sanitaria finalizzata to V.C. and M.R., a Telethon grant GGP06233 to V.C. and a grant from the Interdisciplinary Center of Clinical Research Tübingen (IZKF) to B.W. We are deeply indebted to all DOA patients and their families for participating in this project. Funding to pay the Open Access publication charges for this article was provided by Telethon grant GGP06233.

References

Alexander C, Votruba M, Pesch UEA, Thiselton DL, Mayer S, Moore A, et al. OPA1, encoding a dynamin-related GTPase, is mutated in autosomal dominant optic atrophy linked to choromosome 3q28. Nat Genet 2000; 26: 211–5.

Amati-Bonneau P, Guichet A, Olichon A, Chevrollier A, Viala F, Miot S, et al. OPA1 R445H mutation in optic atrophy associated with sensorineural deafness. Ann Neurol 2005; 58: 958–63.

Amati-Bonneau P, Valentino ML, Reynier P, Gallardo E, Bornstein B, Boissière A, et al. OPA1mutations induce mitochondrial DNA instability and optic atrophy 'plus' phenotypes. Brain 2007; in press.

Atorino L, Silvestri L, Koppen M, Cassina L, Ballabio A, Marconi R, et al. Loss of m-AAA protease in mitochondria causes complex I deficiency and increased sensitivity to oxidative stress in hereditary spastic paraplegia. J Cell Biol 2003; 163: 777–87.

Bonora E, Porcelli AM, Gasparre G, Biondi A, Ghelli A, Carelli V, et al. Defective oxidative phosphorylation in thyroid oncocytic carcinoma is associated with pathogenic mitochondrial DNA mutations affecting complexes I and III. Cancer Res 2006; 66: 6087–96.

Bradford MM. A rapid and sensitive method for the quantitation of microgram quantities of protein utilizing the principle of protein-dye binding. Anal Biochem 1976; 72: 248–54.

Brandt U. Energy converting NADH: quinone oxidoreductase (Complex I). Annu Rev Biochem 2006; 75: 69–92.

Carelli V, La Morgia C, Iommarini L, Carroccia R, Mattiazzi M, Sangiorgi S, et al. Mitochondrial optic neuropathies: how two genomes may kill the same cell type? Biosci Rep 2007; 27: 173–84.

Carelli V, Ross-Cisneros FN, Sadun AA. Mitochondrial dysfunction as a cause of optic neuropathies. Prog Retin Eye Res 2004; 23: 53–89.

Chen H, Chomyn A, Chan DC. Disruption of fusion results in mitochondrial heterogeneity and dysfunction. J Biol Chem 2005; 280: 26185–92.

Cossarizza A, Riva A, Pinti M, Ammannato S, Fedeli P, Mussini C, et al. Increased mitochondrial DNA content in peripheral blood lymphocytes from HIV-infected patients with lipodystrophy. Antivir Therap 2003; 8: 51–57.

Danielson SR, Wong A, Carelli V, Martinuzzi A, Schapira AH, Cortopassi GA. Cells bearing mutations causing Leber's hereditary optic neuropathy are sensitized to Fas-Induced apoptosis. J Biol Chem 2002; 277: 5810–5.

Delettre C, Griffoin J-M, Kaplan J, Dollfus H, Lorenz B, Faivre L, et al. Mutation spectrum and splicing variants in the OPA1 gene. Hum Genet 2001; 109: 584–91.

Delettre C, Lenaers G, Griffoin J-M, Gigarel N, Lorenzo C, Belenguer P, et al. Nuclear gene OPA1, encoding a mitochondrial dynamin-related protein, is mutated in dominant optic atrophy. Nat Genet 2000; 26: 207–10.

DiMauro S, Schon EA. Mitochondrial respiratory-chain diseases. N Engl J Med 2003; 348: 2656–68.

Frezza C, Cipolat S, Martins de Brito O, Micaroni M, Beznoussenko GV, Rudka T, et al. OPA1 controls apoptotic cristae remodeling independently from mitochondrial fusion. Cell 2006; 126: 177–89.

Ghelli A, Zanna C, Porcelli AM, Schapira AH, Martinuzzi A, Carelli V, et al. Leber's hereditary optic neuropathy (LHON) pathogenic mutations induce mitochondrial-dependent apoptotic death in transmitochondrial cells incubated with galactose medium. J Biol Chem 2003; 278: 4145–50.

Griparic L, van der Wel NN, Orozco IJ, Peters PJ, van der Bliek AM. Loss of the intermembrane space protein Mgm1/OPA1 induces swelling and localized constrictions along the lengths of mitochondria. J Biol Chem 2004; 279: 18792–8.

Hollenbeck PJ, Saxton WM. The axonal transport of mitochondria. J Cell Sci 2005; 118: 5411–9.

Hudson G, Amati-Bonneau P, Blakely EL, Stewart JD, He L, Schaefer AM, et al. Mutation of OPA1 causes dominant optic atrophy with external ophthalmoplegia, ataxia, deafness and multiple mitochondrial DNA deletions: a novel disorder of mtDNA maintenance. Brain 2007; in press.

Ishihara N, Fujita Y, Oka T, Mihara K. Regulation of mitochondrial morphology through proteolytic cleavage of OPA1. EMBO J 2006; 25: 2966–77.

Karbowski M, Arnoult D, Chen H, Chan DC, Smith CL, Youle RJ. Quantitation of mitochondrial dynamics by photolabeling of individual organelles shows that mitochondrial fusion is blocked during the Bax activation phase of apoptosis. J Cell Biol 2004; 164: 493–9.

Kim JY, Hwang JM, Ko HS, Seong MW, Park BJ, Park SS. Mitochondrial DNA content is decreased in autosomal dominant optic atrophy. Neurology 2005; 64: 966–72.

King MP, Attardi G. Human cells lacking mtDNA: repopulation with exogenous mitochondria by complementation. Science 1989; 246: 500–3.

Kjer P. Infantile optic atrophy with dominant mode of inheritance: a clinical and genetic study of 19 Danish families. Acta Ophthalmol Scand 1959; 37: 1–146.

Klein JA, Longo-Guess CM, Rossmann MP, Seburn KL, Hurd RE, Frankel WN, et al. The harlequin mouse mutation downregulates apoptosis-inducing factor. Nature 2002; 419: 367–74.

Lee Y, Jeong SY, Karbowski M, Smith CL, Youle RJ. Roles of the mammalian mitochondrial fission and fusion mediators Fis1, Drp1, and Opa1 in apoptosis. Mol Biol Cell 2004; 15: 5001–11.

Lodi R, Tonon C, Valentino ML, Iotti S, Clementi V, Malucelli E, et al. Deficit of in vivo mitochondrial ATP production in OPA1-related dominant optic atrophy. Ann Neurol 2004; 56: 719–23.

Nijtmans LG, Henderson NS, Holt IJ. Blue Native electrophoresis to study mitochondrial and other protein complexes. Methods 2002; 26: 327–34.

Ogilvie I, Kennaway NG, Shoubridge EA. A molecular chaperone for mitochondrial complex I assembly is mutated in a progressive encephalopathy. J Clin Invest 2005; 115: 2784–92.

Olichon A, Baricault L, Gas N, Guillou E, Valette A, Belenguer P, et al. Loss of OPA1 perturbates the mitochondrial inner membrane structure and integrity, leading to cytochrome c release and apoptosis. J Biol Chem 2003; 278: 7743–6.

Olichon A, Elachouri G, Baricault L, Delettre C, Belenguer P, Lenaers G. OPA1 alternate splicing uncouples an evolutionary conserved function in mitochondrial fusion from a vertebrate restricted function in apoptosis. Cell Death Differ 2007a; 14: 682–92.

Olichon A, Emorine LJ, Descoins E, Pelloquin L, Brichese L, Gas N, et al. The human dynamin-related protein OPA1 is anchored to the mitochondrial inner membrane facing the inner-membrane space. FEBS Lett 2002; 523: 171–6.

Olichon A, Guillou E, Delettre C, Landes T, Arnaune-Pelloquin L, Emorine LJ, et al. Mitochondrial dynamics and disease, OPA1. Biochim Biophys Acta 2006; 1763: 500–9.

Olichon A, Landes T, Arnauné-Pelloquin L, Emorine LJ, Mils V, Guichet A, et al. Effects of OPA1 mutations on mitochondrial morphology and apoptosis: relevance to ADOA pathogenesis. J Cell Physiol 2007b; 211: 423–30.

Payne M, Yang Z, Katz BJ, Warner JE, Weight CJ, Zhao Y, et al. Dominant optic atrophy, sensorineural hearing loss, ptosis, and ophthalmoplegia: a syndrome caused by a missense mutation in OPA1. Am J Ophthalmol 2004; 138: 749–55.

Pesch UE, Leo-Kottler B, Mayer S, Jurklies B, Kellner U, Apfelstedt-Sylla E, et al. OPA1 mutations in patients with autosomal dominant optic atrophy and evidence for semi-dominant inheritance. Hum Mol Genet 2001; 10: 1359–68.

Robinson BH, Petrova-Benedict R, Buncic JR, Wallace DC. Nonviability of cells with oxidative defects in galactose medium: a screening test for affected patient fibroblasts. Biochem Med Metab Biol 1992; 48: 122–6.

Schimpf S, Schaich S, Wissinger B. Activation of cryptic splice sites is a frequent splicing defect mechanism caused by mutations in exon and intron sequences of the OPA1 gene. Hum Genet 2006; 118: 767–71.

Sesaki H, Southard SM, Yaffe MP, Jensen RE. Mgm1p, a dynamin-related GTPase, is essential for fusion of the mitochondrial outer membrane. Mol Biol Cell 2003; 14: 2342–56.

Srere P.A. Citrate synthase. Methods Enzymol 1969; 13: 3–10.

Ugalde C, Vogel R, Huijbens R, Van Den Heuvel B, Smeitink J, Nijtmans L. Human mitochondrial complex I assembles through the combination of evolutionary conserved modules: a framework to interpret complex I deficiencies. Hum Mol Genet 2004; 13: 2461–72.

Vahsen N, Cande C, Briere JJ, Benit P, Joza N, Larochette N, et al. AIF deficiency compromises oxidative phosphorylation. EMBO J 2004; 23: 4679–89.

Vogel RO, Janssen RJ, Ugalde C, Grovenstein M, Huijbens RJ, Visch HJ, et al. Human mitochondrial complex I assembly is mediated by NDUFAF1. FEBS J 2005; 272: 5317–26.

Youle RJ, Karbowski M. Mitochondrial fission in apoptosis. Nat Rev Mol Cell Biol 2005; 8: 657–63.

Zanna C, Ghelli A, Porcelli AM, Martinuzzi A, Carelli V, Rugolo M. Caspase-independent death of Leber's hereditary optic neuropathy cybrids is driven by energetic failure and mediated by AIF and Endonuclease G. Apoptosis 2005; 10: 997–1007.